This article has been accepted for publication in a future issue of this journal, but has not been fully edited. Content may change prior to final publication. Citation information: DOI 10.1109/JLT.2019.2920680, Journal of Lightwave Technology

Numerical and Experimental Characterization of Radiation Mode of 45° Tilted Fiber Grating

Huabao Qin, Qinyun He, Zhikun Xing, Xi Guo, Zhijun Yan, Qizhen Sun, Kaiming Zhou, Hushan Wang, Deming Liu and Lin Zhang

***Abstract*—In this paper, we have numerically and experimentally investigated the radiation mode of 45° tilted fiber grating (45° TFG). By introducing the axial distributions into the volume current method, we have established a three-dimension theoretical model to analyze spatial distributions of the radiation mode of 45° TFG, and measured the radiation mode spatial distributions in experiment. Both numerical and experimental results show that the radiation mode of 45° TFG exhibits an exponential reduction along the fiber axial direction, and a quasi-Gaussian profile along the radial direction of fiber. Additionally, we have also measured the detailed polarization dependent azimuthal intensity distributions of radiation modes of both s- and p-polarized core modes. The degree of polarization (DOP) of radiation mode is around 99.886%, which is independent of the length and the polarization extinction ratio (PER) of the grating. Moreover, for the first time, we have experimentally observed a very weak p-polarized component existing in the radiation mode, which has matched well with the simulation results.**

***Index Terms*—Fiber optics, Fiber gratings, Radiation, Polarization, Exponential distribution.**

I. Introduction

SINCE the first fiber grating was proposed by K. Hill in 1978 [1], the properties of fiber grating have been systemically investigated and the theories have been well established after decades of development. Among the various fiber gratings, there is a special kind of grating with blazed grating structure firstly reported by Meltz [2], called tilted fiber grating (TFG). Due to its unique mode conversion characteristics, the TFGs have attracted much deserved attention in recent years and have been widely applied in fiber sensing and communication areas. According to the different mode coupling behaviors, TFGs can be classified into three different types, including the backward cladding mode coupling tilted fiber Bragg grating (TFBG), forward cladding mode coupling excessively tilted fiber grating (Ex-TFG) and radiation mode coupling 45° tilted fiber grating (45°TFG). Due to the asymmetric grating structure, the TFBG and Ex-TFG indicate excellent polarization related cladding mode coupling behaviors, which have been used as in-fiber twist sensor, fiber based surface plasma resonance sensor, refractive index sensor, liquid surface tension sensor, magnetic field sensor, electrochemical and biochemical sensor [3]-[12]. And the TFGs with the tilt angle between 23.1° and 66.9° with respect to the normal direction of fiber axis can radiate the light out of fiber core with very strong polarization correlation. However, only the grating with a tilt angle of 45° can directly and effectively tap the s-polarized light out of fiber core and leave the p-polarized light traveling through the grating. Due to such unique polarization characteristics, 45° TFGs have been applied as ideal in-fiber linear polarizers and integrated polarizer [13]-[15]. On the other hand, the radiation mode has also attracted much attention. So far, 45° TFG has been successfully applied as a key element to separate polychromatic light into monochromatic components in optical spectrum analyzer, wireless optical communication system, spectrally encoded imaging system, ultrafast photonic time-stretch imaging system and Fourier-domain optical coherence tomography (OCT) spectrometer [16]-[19]. However, different from the traditional volume diffraction gratings, the spatial distributions of the radiation mode of a uniform 45° TFG have several inherent flaws, such as the asymmetrical energy distributions and the large divergence angle. So, the complicated optical modules are needed to compensate the performance degradation, which have limited the further improvements of the systems. To overcome these drawbacks, it is necessary to analyze the characteristics of the radiation mode of 45° TFG. There are several theories that have been proposed to analyze the mode coupling properties of TFGs. T. Erdogan has used the coupled mode theory (CMT) to analyze the radiation mode coupling behaviors of the TFGs [20],[21]. R. Kashyap has proposed a model to analyze the properties of the sidetap grating filters based on antenna theory [22]. However, these two models are not focused on the radiation field of TFG and they haven't explained the distribution characteristics of the

This work is supported by National Natural Science Foundation of China (No. 61505244) and the Fundamental Research Funds for the Central Universities, HUST: 2017KFYXJJ033; the Science Fund for Creative Research Groups of the Nature Science Foundation of Hubei (NO. 2018CFA004), the Major Projects of Technical Innovation of Hubei (NO. 2018AAA040).

H. Qin, Q. He, Z. Xing, X. Guo, Z. Yan, Q. Sun, and D. Liu are with the School of Optical and Electronic Information, National Engineering Laboratory for Next Generation Internet Access System, Huazhong University of Science and Technology, Wuhan 430074, Hubei, P. R. China (e-mail: yanzhijun@gmail.com;).

K. Zhou and L. Zhang are with the Aston Institute of Photonic Technologies, Aston University, Birmingham, B4 7ET, U.K., and K. Zhou is also with the State Key Laboratory of Transient Optics and Photonics.

H. Wang is with the State Key Laboratory of Transient Optics and Photonics, Xi'an Institute of Optics and Precision Mechanics, Chinese Academy of Sciences, Xi'an 710119, China

This article has been accepted for publication in a future issue of this journal, but has not been fully edited. Content may change prior to final publication. Citation information: DOI 10.1109/JLT.2019.2920680, Journal of Lightwave Technology

radiation mode of a TFG. In 2001, Li *et al*. used volume current method (VCM) to analyze the characteristics of the radiation mode of TFG and compared the results with the CMT [23],[24]. Walker *et al*. have discussed the parametric dependencies of the radiation patterns of TFBG based on VCM [25]. But they only applied the transverse far-field approximation and their models could not accurately describe the distribution of the radiation mode in longitudinal dimension. In 2003, C. Jauregui proposed a near-field theoretical model to analyze the radiated field of the TFG with 34°tilt angle [26],[27]. S. Jian *et al*. proposed a simplified CMT and a full vector complex CMT for the analysis of radiation mode coupling of TFGs [28],[29]. In 2012, T. Yoshino used beam tracing approach to investigate the polarization properties of the TFG polarizer [30]. In 2014, J. Albert *et al*. experimentally investigated the radiation pattern of a 10° TFBG under a microscope [31]. However, there are few papers that have systematically investigated the radiation mode of 45° TFG in theory and experiment. In this paper, we have proposed a comprehensive theoretical model to analyze the properties of the radiation mode of 45° TFG. In addition, we have characterized the radiation mode properties of 45° TFG in the experiment. The spatial distributions and the polarization characteristics of the radiation mode have been investigated. Furthermore, we also have observed that the 45° TFG could excite very weak p-polarized radiation mode comparing with the s-polarized one, which shows a good match between the proposed theoretical model and the experiment results.

II. Theoretical Analysis of Radiation Mode

Among the various theoretical analysis methods, Li *et al*. used VCM to analyze the characteristics of the radiation mode of TFG and achieved good results. Compared with the other methods, VCM can intuitively analyze and explain the properties of the radiation mode of TFG. Based on VCM, the grating structure of TFG is regarded as the period perturbations of the refractive index, which would induce perturbed electric and magnetic fields. By using the Maxwell's equations, the induced perturbations of grating can be derived. The power-flow density vector of the field induced by the perturbations of grating can indicate the intensity of the radiation pattern of TFG, which can be expressed as [23]:

$$\left.\begin{aligned} S &= \frac{\pi c\varepsilon_0 n_0^2 \delta n^2 k_0^3 E_0^2}{4r}\left(\frac{\Delta^2}{k_0^2 n_0^2}+\frac{k_t^2}{k_0^2 n_0^2}\sin^2(\delta-\phi)\right)F^2 \\ F &= \frac{K_s a J_0(ua)J_1(K_s a)-uaJ_1(ua)J_0(K_s a)}{K_s{}^2-u^2} \end{aligned}\right\} \quad (1)$$

where n_0 is the refractive index of the fiber core, δn is the modulated refractive index induced by ultraviolet light exposure, a is the radius of fiber core, $k_0=2\pi/\lambda_0$ is the wave vector of the incident light, E_0 is the intensity of the electric field, β is the propagation constant, r is the radius of the fiber core, $\Delta=\beta-K_g$, $K_g=2\pi\cos\theta/\Lambda$ and $K_t=2\pi\sin\theta/\Lambda$ represent the longitudinal and transverse wavenumbers of the grating, respectively, where Λ is the period of grating and θ is the tilted angle, $k_t=\sqrt{k_0^2 n_0^2-(\beta-K_g)^2}$ is the projection of the wave vector of emergent light in transverse direction, δ and ϕ are the polarization and azimuthal angle of the radiated light, respectively, $K_s=\sqrt{k_t^2+K_t^2-2k_t K_t\sin\phi}$ is the mismatching among the wave vectors of grating, incident light and emergent light, and u is the waveguide parameter of fiber and J is the Bessel function.

Here, Eq. 1 illustrates the azimuthal distributions of the radiation mode, but lacks the axial distribution information. To better analyze the radiation properties of TFG, the axial information needs to be introduced into the VCM. In this paper, we provide a simple but efficient method to analyze the behaviors of radiation mode along the fiber axis and propose a comprehensive theoretical model for describing the radiation mode of TFG.

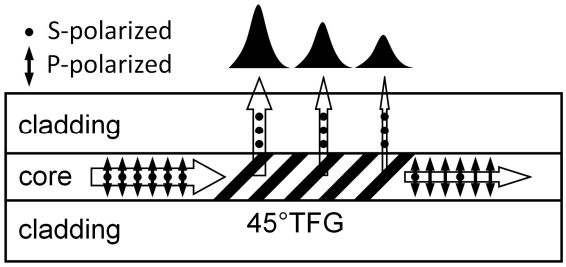

Fig. 1. Schematic diagram for analyzing the distribution along the fiber.

Due to the irreversible radiation behavior of TFG, the grating structure can be divided into sub-sections along the fiber axis with the same structure, and the radiation pattern of the whole grating is the sum of the patterns of each sub-section, as illustrated in Fig. 1. The transverse distributions of radiation mode for each sub-section can be figured out by using the VCM. However, when the light of core mode transmits through each sub-section, the radiation would cause energy attenuation of light, resulting in the decrement of the electric field intensity of incident light. When the sub-sections are small enough, the intensity of the radiation mode can be expressed as:

$$I_R = \frac{1}{T}\int_0^T\left(\oint S d\phi\right)dt = \alpha I_0 \quad (2)$$

where α is the coupling coefficient between the core mode and the radiation mode and I_0 is the intensity of the incident light. The intensity distribution of radiation mode along the fiber axis can be written as:

$$I(z) = \alpha(1-\alpha)^{\frac{z}{\Lambda}-1} I_0 \quad (3)$$

and α is

$$\alpha = \frac{\pi n_0^2 \delta n^2 a^2 k_0^3}{2r}\oint(\cos^2\theta_r+\sin^2\theta_r\sin^2(\delta-\phi)) \cdot\left(\frac{K_s J_0(ua)J_1(K_s a)-uJ_1(ua)J_0(K_s a)}{K_s{}^2-u^2}\right)^2 d\phi \quad (4)$$

where θ_r is the emergent angle of the radiated light, which is related to the wavelength of the incident light, and z is the axial position of grating.

Therefore, the spatial distributions of the radiation mode of TFG can be rewritten as:

This article has been accepted for publication in a future issue of this journal, but has not been fully edited. Content may change prior to final publication. Citation information: DOI 10.1109/JLT.2019.2920680, Journal of Lightwave Technology

$$\left.\begin{aligned} I(r,\phi,z) &= \frac{c\varepsilon_0\pi^2 E_0^2 n_0^4 \delta n^4 a^4 k_0^6}{8r^2}(1-\alpha)^{\frac{z}{\Lambda}-1} \\ &\cdot(\cos^2\theta_r + \sin^2\theta_r \sin^2(\delta-\phi))F^2(\phi)G(\phi) \\ F(\phi) &= \frac{K_s(\phi)J_0(ua)J_1(K_s(\phi)a)}{K_s^2(\phi)-u^2} - \\ &\frac{uJ_1(ua)J_0(K_s(\phi)a)}{K_s^2(\phi)-u^2} \\ G(\phi) &= \oint(\cos^2\theta_r + \sin^2\theta_r \sin^2(\delta-\phi))\cdot F(\phi)^2 d\phi \end{aligned}\right\} \quad (5)$$

The formula contains two part: the azimuthal distribution mainly described by $F^2(\phi)G(\phi)$ and the axial distribution described by $(1-\alpha)^{z/\Lambda-1}$, the latter indicates the spatial distributions of the radiation mode of TFG. For a uniform TFG, which has a constant modulation of the refractive index, the radiation mode would have a negative exponential distribution along the fiber axis according to Eq. 5. The equation gives a simplified but intuitional and comprehensive explanation for describing the characteristics of the radiation mode of TFG, and further discussions will be presented in the next section.

III. Radiation Mode Characteristics of 45° TFG and Discussions

In this section, we have analyzed the characteristics of 45° TFG with numerical simulation and experiment. A simulated three-dimension distribution pattern of the radiation mode of 45° TFG has been carried out for the first time. The radiation modes have been captured and the distributions of the mode have been measured in the experiment.

A. Simulation results

The spatial distributions of the radiation mode of 45° TFG have been numerically simulated with the proposed model. In the simulation, the refractive index of fiber core was set as 1.448, the wavelength was set as 1550nm and the magnitude of E was considered to be 1. The radius of the core was set to be 4.5 μm, the grating period and tilted angle were set as 748 nm and 45°, respectively, and the induced index perturbation was set as 0.001. The simulated results of the azimuthal distributions with two orthogonal polarization states and the 3D distribution pattern of the radiation mode are depicted in Fig. 2 a, b and c, respectively.

As shown in Fig. 2a, the patterns of s-polarized radiation mode have a Gaussian profile with several side lobes. The energy is mainly distributed within around 20° azimuthal angles ranging from 80° to 100°, where about 99.5% of the energy is contained in this region, and the intensity reaches the maximum at 90°. There are many side lobes that exhibit an attenuation of periodic oscillation in logscale. The difference of the intensity between the main lobe and the first side lobe is about 25dB, as seen in Fig. 2b. For the p-polarized radiation mode, it shows the same periodic oscillation attenuation as the p-polarized one. However, in the azimuthal angle region between 80° and 100°, there are two lobes instead of one main lobe. The intensity of the p-polarized radiation mode is about 26dB weaker than the s-polarized one, and reaches the minimum at 90°, which is the major difference between these two modes. Therefore, only few p-polarized radiation modes could be radiated by TFG. By using Eq. 5, we have simulated the whole spatial distributions of the radiation mode of 45° TFG (see Fig. 2c). The s-polarized radiation mode of 45° TFG shows an exponential reduction along the grating axis and has a Gaussian profile at the azimuthal direction of the fiber.

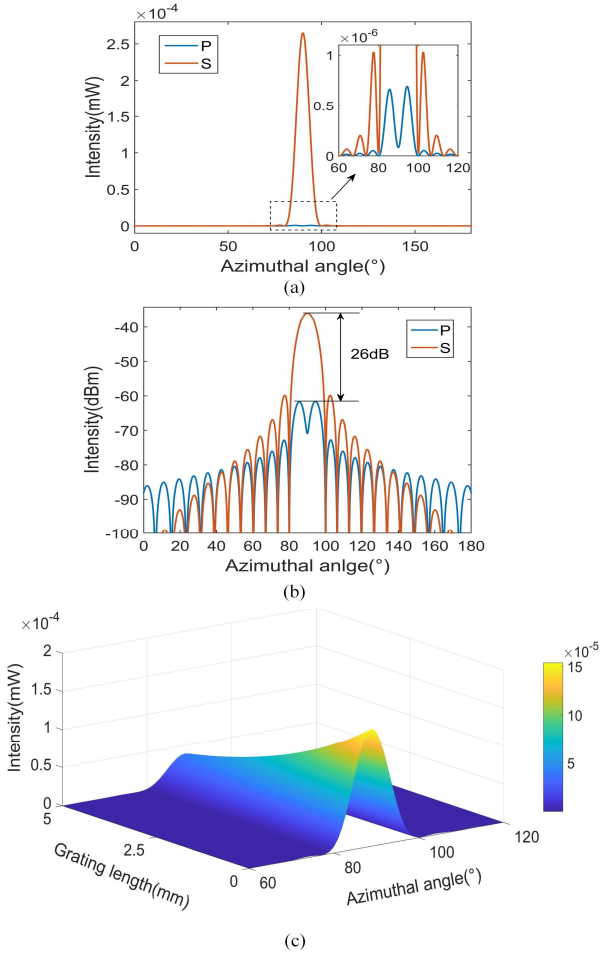

Fig. 2. Simulated azimuthal distributions of the radiation mode in (a) linescale and (b) logscale; (c) the simulated 3D distribution pattern of the radiation mode (s-polarized).

B. Spatial distributions of the radiation mode

To verify the simulation results, we have experimentally measured the radiation mode of 45° TFG in terms of the distribution profile and the intensity distributions along the fiber axial and azimuthal directions.

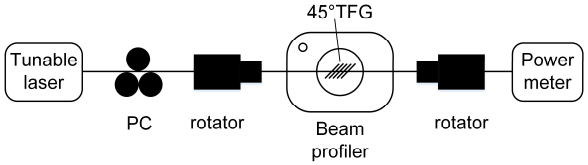

Fig. 3. Experimental setup for capturing the radiated light by the radiation mode of 45° TFG.

This article has been accepted for publication in a future issue of this journal, but has not been fully edited. Content may change prior to final publication. Citation information: DOI 10.1109/JLT.2019.2920680, Journal of Lightwave Technology

The experimental setup is indicated in Fig. 3, which includes a tunable laser, polarization controller (PC), beam profiler (Gentec-EO Beamage-4M-IR), optical power meter and fiber rotators. In the experimental setup, the wavelength of the laser is set to be 1550nm, the PC is used to control the polarization state of light launched into 45° TFG. By employing the power meter, we can confirm which polarization state of light has passed through the grating (the maximum value in power meter shows that the p-polarized light has been launched into the grating; conversely, the minimum value in power meter shows that the s-polarized light has been launched into the grating). Three 45° TFGs with different grating lengths (5mm, 10mm, 15mm) and polarization extinction ratios (PER) (3.24dB, 5.42dB, 9.77dB) have been investigated in the experiment. These three grating are fabricated with the same phase mask and they have the same period of 748nm, but the exposure lengths have been controlled to be 5, 10 and 15mm, respectively.

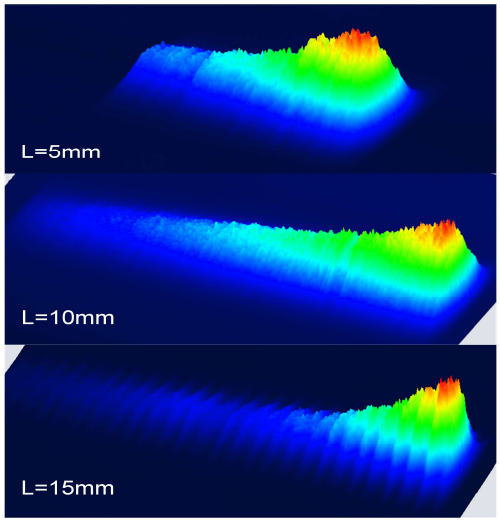

Fig. 4. The captured radiation patterns of the 45° TFGs with different grating lengths.

With the proper adjustments of polarization state and the collimation of the radiation direction, the radiation patterns of 45° TFGs have been captured and shown in Fig. 4. The captured patterns present similar distribution profiles of radiated light with the simulation results in Fig. 2c, in which the maximum intensity appears at the beginning of the grating and exponentially decreases along the fiber axis. Since the effective length of the CCD is only about 11.26mm, the radiation pattern of the 15mm-long grating is incompletely captured by the beam profiler.

For detailed analysis, the profiles of the radiation patterns along *x*- (fiber axis) and *y*- (fiber cross-section) axes have been extracted and compared with the simulation results. As shown in Fig. 5a, the distributions of radiation mode along y-axis show a Gaussian profile and are in good agreement with the simulation results. The minor differences between the simulation and experimental results are caused by the non-uniform response of each pixel of the beam profiler.

In addition, as shown in Fig. 5b-d, the intensity distributions of the radiation modes are reduced exponentially along the fiber axial direction. The lengths of the profiles are in accord with the actual lengths of gratings, and the calculated coupling coefficients are around 9.973×10^{-4}, 6.591×10^{-4} and 1.073×10^{-3}, respectively, for the three measured 45° TFGs. The larger the coupling coefficients represent the stronger ability of the grating to couple more s-polarized components of the incident light into radiation mode, which is related to the correlation between the PER and the length of the grating. Eventually, both the results of the exponentially reducing distributions and the different coupling coefficients have preliminarily verified that the proposed model can well describe the axial distribution characteristics of the radiation mode of 45° TFG.

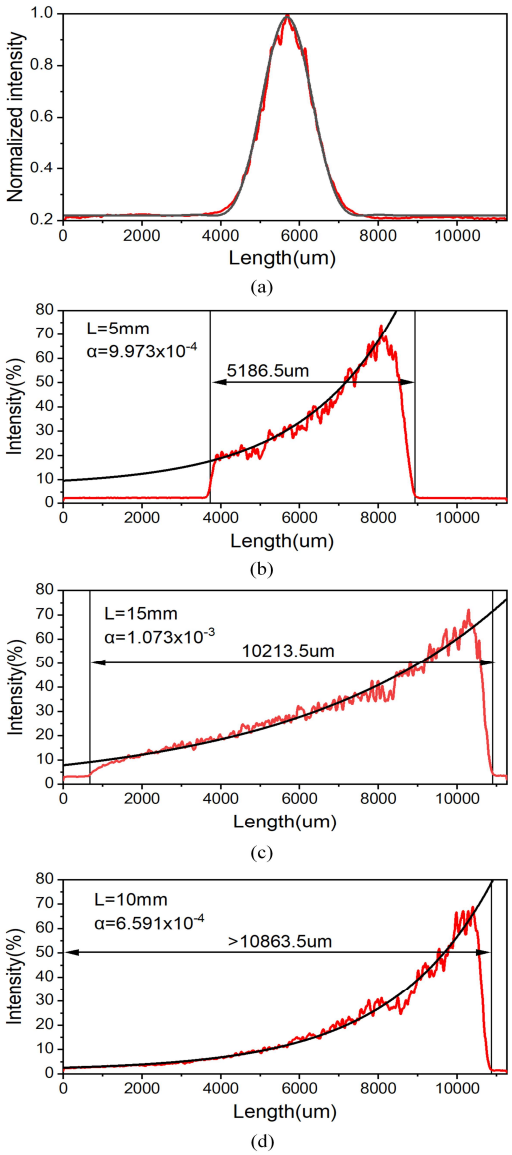

Fig. 5. The simulation (black curves) and experimental (red curves) results of radiation mode distributions along (a) azimuthal direction and axial direction with the grating lengths of (b) 5mm, (c) 10 mm and (d) 15 mm, respectively.

Because of the sensitivity and background noise limitations of CCD, the radiation patterns captured by the beam profile only contain the intensity distribution information along fiber

This article has been accepted for publication in a future issue of this journal, but has not been fully edited. Content may change prior to final publication. Citation information: DOI 10.1109/JLT.2019.2920680, Journal of Lightwave Technology

grating, and the detailed distributions along the azimuthal direction could not be observed. For further analysis, we built another experimental setup to observe the azimuthal distributions of the radiation mode with a high-sensitivity photodetector (PD), see in Fig. 6. The PD is fixed on a rotary stage which can facilitate the fiber rotation from 0° to 360°, and the grating is set at the center of the stage. Here, the PC and power meter are used to confirm the polarization state of the radiation mode. In this experiment, we have measured the azimuthal distributions of the radiation mode of 45° TFG with s- and p-polarization in detail, and the measurement results are illustrated in Fig. 7.

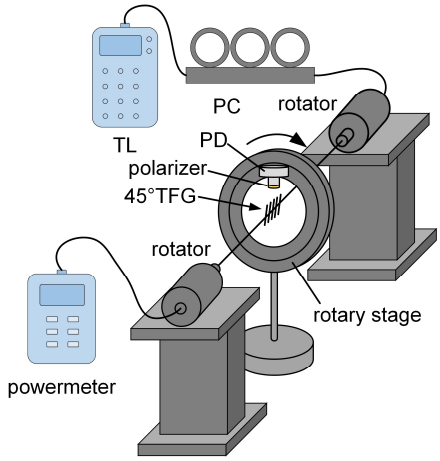

Fig. 6. Experimental setup for measuring the detailed azimuthal distribution of the radiation mode.

Figure 7a shows the azimuthal distributions of the radiation mode of 45° TFG with a 2° measuring step, and it is clear that the distribution profiles are not similar to Gaussian profiles. There are two "shoulders" on both sides of the main lobe, which makes the profile different from the previous results in Fig. 5a. It is worth mentioning that a small spindle tail with a shape similar to the main lobe occurs in the opposite direction of the radiation mode. The intensity of the tail is about 16.15dB weaker than the main lobe. It is reasonable to regard it as the results of the Fresnel reflection at the interface between fiber and air. In addition, the effect of the polarization state of radiation mode has also been considered. According to the simulation results, the intensity of the p-polarized radiation mode should be much weaker than the s-polarized one. However, the radiated energy of the p-polarized radiation mode could still be measured, and the results are illustrated in Cartesian coordinate and polar coordinate system, respectively, as shown in Fig. 7a and 7b. Compared with the radiation mode of s-polarized component, the intensity of p-polarized radiation mode is much lower, with a difference of about 26.23dB. The distributions of p-polarized radiation mode show a profile similar to the s-polarized radiation mode, as there is a main lobe and two side lobes. However, according to the simulation results, there should be two lobes instead of the main lobe.

In our theory, the difference is caused by the non-single polarization state of the incident light. The incident light was fully p-polarized during the simulation. However, during the experiment, due to the limitations of the degree of polarization of tunable laser and the adjustments of the PC, the polarization state of the incident light is not completely p-polarized, and there are still few s-polarized components in the excited radiation mode. Because of the huge difference of the coupling efficiency between these two polarized radiation modes, even a very small s-polarized component in the incident light could still excite the radiation mode with nearly equal strength to the p-polarized component. So, we could not observe the distinctive two lobes of the p-polarized radiation mode, which have been submerged in the main lobe of the excited s-polarized radiation mode profile. The measured results are considered to be the combination intensity profile of p-polarized and s-polarized radiation modes.

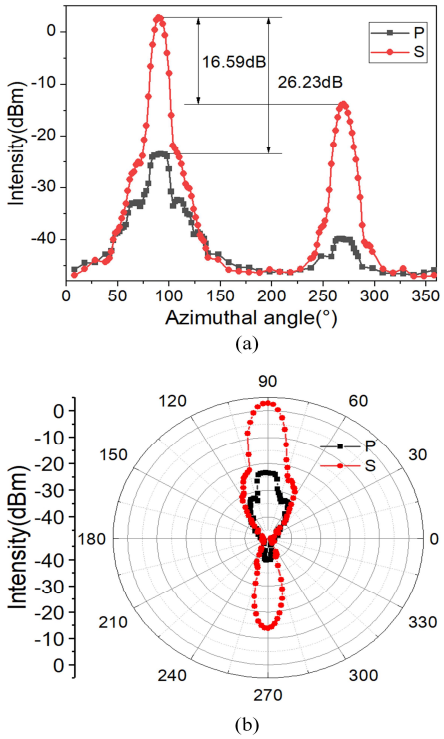

Fig. 7. The azimuthal distributions of s-polarized and p-polarized radiation modes in (a) Cartesian coordinate and (b) polar coordinate system.

To eliminate the effects of the undesired polarization state in the radiation mode, we put a polarizer at the front of PD as a filter. The polarizer has been rotated in two orthogonal directions corresponding to each polarization state. The measured and the simulation results of the radiation modes are plotted in Fig. 8a and b, respectively. With the employment of the polarizer, the polarization crosstalk has been effectively eliminated, and much clearer profiles of the radiation mode have been observed. As shown in Fig. 8a, the divergence angle of the s-polarized radiation mode is about 12°, showing that 45° TFG has a good potential to act as a polarization-dependent light source in fiber communication and OCT areas. As illustrated in the figure, the two "shoulders" have expanded the width of the pattern from 12° to 32°, where the main lobe occupies around 95.05% energy of the whole radiation mode. From the comparison between the simulation and experimental

This article has been accepted for publication in a future issue of this journal, but has not been fully edited. Content may change prior to final publication. Citation information: DOI 10.1109/JLT.2019.2920680, Journal of Lightwave Technology

results, it is found that the "shoulders" are the first side lobes of the radiation mode. Actually, they are the characteristic features of the simulation results, which make the profile of the pattern different from the traditional Gaussian distribution. More importantly, the splitting lobes of the p-polarized radiation mode have been successfully measured and illustrated in Fig. 8b. The dip of the p-polarized radiation mode occurs at 90° as expected. There is a slight difference between the intensity of two lobes, which might be caused by the mismatching between the incident light and the grating structure. However, the most significant features of both s- and p-polarized radiation modes have been observed and the experimental results match well with the simulated results, which have further verified the reliability of the proposed theoretical model.

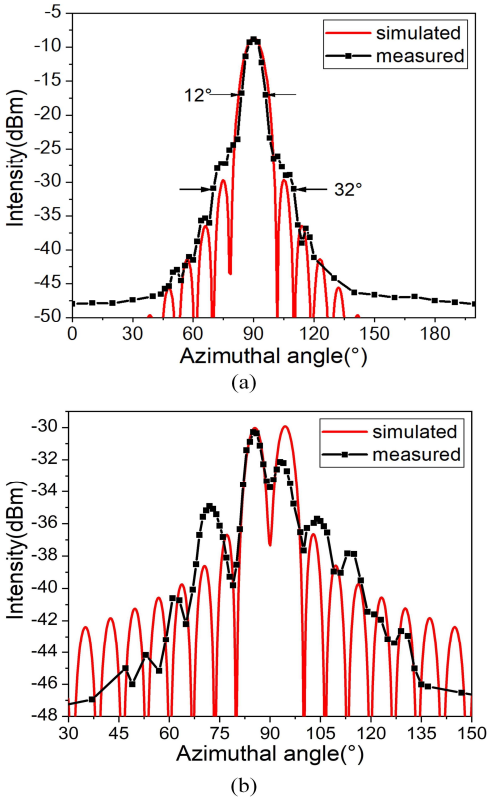

Fig. 8. The filtered results and the simulated results of the distributions of (a) s-polarized and (b) p-polarized radiation modes.

C. *Polarization distributions of the radiation mode*

According to the simulation results, the radiation mode of 45° TFG should mainly contain the s-polarized components and very few p-polarized components of the light. We have also measured the polarization distributions of the radiation mode of 45° TFG with different PERs (seen in Fig. 9a). The polarization distributions of different radiation modes have the same letter "8" distribution pattern and the degree of polarization (DOP) of the modes is around 99.886%. The perfect letter "8" distribution pattern indicates that the radiation mode is purely linearly polarized, while the DOP of the radiation mode is independent of the PER of the grating. In addition, we have launched the p-polarized light into the grating and measured the polarization distributions of the excited radiation mode, which are shown in Fig. 9b. The profile of the distributions has a letter "8" shape similar to the s-polarized, but the intensity is much lower and the DOP drops to 91.044%. Besides, the polarization angle of the excited radiation mode has diverged from the normal direction for about 10° according to the experimental results. This result has further proved that both s- and p-polarized components are existed in the excited radiation mode and the polarization state has been affected by the mixture of different polarized components. So, the excited radiation mode for the p-polarized incident light consists of a major s-polarized component and a very little p-polarized component. According to the experimental results, the radiation mode excited by p-polarized incident light only has around 10 percent (or less) of p-polarized component, in accord with the previous conclusion. Overall, the experimental results also verify that the 45° TFGs have a strong polarized property and a single polarization radiation feature.

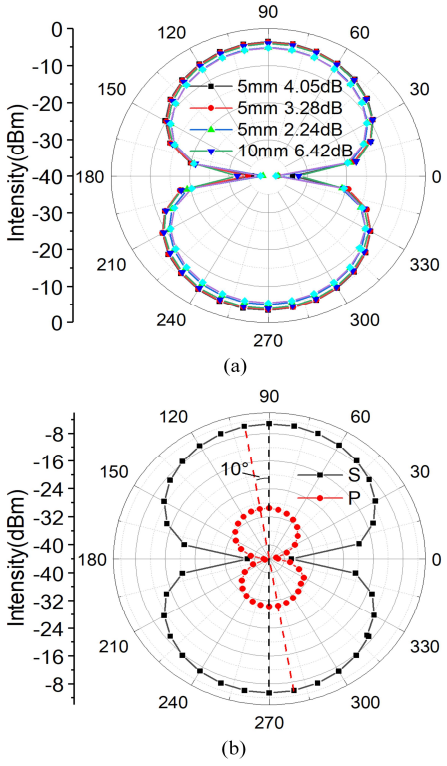

Fig. 9. (a) the polarization distributions of the radiation mode with different grating lengths and different PERs; (b) the polarization distributions of different polarized radiation modes for a 5-mm long and 4dB PER 45° TFG.

IV. Conclusion

In conclusion, we have theoretically analyzed the distributions of the radiation mode of 45° TFG along the fiber axial direction and proposed a three-dimension model for describing the spatial distributions of the radiation mode. The simulation results of the model for a uniform 45° TFG show that the radiation mode presents a quasi-Gaussian profile at the azimuthal direction in linear scale, while in axial direction it is an exponential reduction. Also, the reduction rate is related to the coupling coefficient of 45° TFG. A simulated 3D radiation

pattern of a 5-mm long 45° TFG has been obtained. The actual patterns of the radiation modes for gratings with different grating lengths have been captured and analyzed. The results show that the energy is mainly distributed at the front of the grating and gradually reduced in an exponential function along the fiber axis. Despite of the different lengths of grating, the reduction shows a similar trend. In addition, we have measured the azimuthal intensity distributions of 45° TFG in logscale and analyzed the characteristics of the radiation mode in detail. The experimental results show a good agreement with the simulation results, verifying the validity of the theoretical model. The polarization distributions of the radiation mode indicate that the radiated light is a perfect linear polarized light, of which the DOP is about 99.886% and is independent of the length and PER of the grating. In addition, we have experimentally demonstrated that 45° TFG could excite the p-polarized radiation mode, according to the measured intensity distributions and the deviation of the polarization angle. Together with its unique characteristics of the radiation mode, 45° TFG may be a desirable in-fiber device in polarization-related spectroscopy analysis, optical wireless communication and spectral imaging areas.

REFERENCES

[1] K. Hill, Y. Fujii, D. C. Johnson, and B. Kawasaki, "Photosensitivity in optical fiber waveguides: Application to reflection filter fabrication," *Appl. Phys. Lett*., vol. 32, no. 10, pp. 647-649, 1978.

[2] G. Meltz, W. W. Morey, and W. H. Glenn, "In-fiber Bragg grating tap," in *Optical Fiber Communication*, San Francisco, California, 1990, p. TUG1.

[3] J. Lao, P. Sun, F. Liu, X. Zhang, C. Zhao, W. Mai, T. Guo, G. Xiao, J. Albert, "In situ plasmonic optical fiber detection of the state of charge of supercapacitors for renewable energy storage. " *Light: Sci. Appl*., vol. 7, no. 1, pp. 34, 2018.

[4] X. Chen, J. Xu, X. Zhang, T. Guo, and B. O. Guan, "Wide range refractive index measurement using a multi-angle tilted fiber Bragg grating," *IEEE Photon Technol. Lett.*, vol. 29, no. 9, pp. 719-722, 2017.

[5] Z. Liu, C. Shen, Y. Xiao, J. Gong, J. Wang, T. Lang, C. Zhao, C. Huang, Y. Jin, and X. Dong, "Liquid surface tension and refractive index sensor based on a tilted fiber Bragg grating," *J. Opt. Soc. Am. B: Opt. Phys*., vol. 35, no. 6, pp. 1282-1287, 2018.

[6] T. Guo, F. Liu, B.O. Guan, J. Albert, "Tilted fiber grating mechanical and biochemical sensors, " *Opt. Laser Technol*., vol. 78, pp. 19-33, 2016.

[7] J. Albert, L. Y. Shao, and C. Caucheteur, "Tilted fiber Bragg grating sensors," *Laser Photonics Rev.*, vol. 7, no. 1, pp. 83-108, 2013.

[8] J. Zheng, X. Dong, P. Zu, L. Y. Shao, C. C. Chan, Y. Cui, and P. P. Shum, "Magnetic field sensor using tilted fiber grating interacting with magnetic fluid," *Opt. Express*, vol. 21, no. 15, pp. 17863-17868, 2013.

[9] C. Shen, C. Zhong, D. Liu, X. Lian, J. Zheng, J. Wang, Y. Semenova, G. Farrell, J. Albert, and J. F. Donegan, "Measurements of milli-Newton surface tension forces with tilted fiber Bragg gratings," *Opt. Lett.*, vol. 43, no. 2, pp. 255-258, 2018.

[10] T. Guo, F. Liu, X. Liang, X. H. Qiu, Y. Y. Huang, C. Xie, P. Xu, W. Mao, B. O. Guan, and J. Albert, "Highly sensitive detection of urinary protein variations using tilted fiber grating sensors with plasmonic nanocoatings, " *Biosens. Bioelectron*., vol. 78, pp. 221-228, 2016.

[11] B. Luo, Y. Xu, S. Wu, M. Zhao, P. Jiang, S. Shi, Z. Zhang, Y. Wang, L. Wang, and Y. Liu, "A novel immunosensor based on excessively tilted fiber grating coated with gold nanospheres improves the detection limit of Newcastle disease virus," *Biosens. Bioelectron*., vol. 100, pp. 169-175, 2018.

[12] X. Chen, K. Zhou, L. Zhang, and I. Bennion, "In-Fiber Twist Sensor Based on a Fiber Bragg Grating With 81° Tilted Structure," *IEEE Photon Technol. Lett*., vol. 18, no. 24, pp. 2596-2598, 2006.

[13] Z. Yan, C. Mou, K. Zhou, X. Chen, and L. Zhang, "UV-inscription, polarization-dependant loss characteristics and applications of 45° tilted fiber gratings," *J. Lightwave Technol.*, vol. 29, no. 18, pp. 2715-2724, 2011.

[14] G. Bharathan, D. D. Hudson, R. I. Woodward, S. D. Jackson, and A. Fuerbach, "In-fiber polarizer based on a 45-degree tilted fluoride fiber Bragg grating for mid-infrared fiber laser technology," *OSA Continuum,* vol. 1, no. 1, pp. 56-63, 2018.

[15] M. T. Posner, N. Podoliak, D. H. Smith, P. L. Mennea, P. Horak, C. B. Gawith, P. G. Smith, and J. C. Gates, "Integrated polarizer based on 45° tilted gratings," *Opt. Express,* vol. 27, no. 8, pp. 11174-11181, 2019.

[16] K. Zhou, X. Chen, Z. Yan, A. Adebayo, and L. Zhang, "Optical spectrum analyzer using a 45° tilted fiber gating," in *Advanced Photonics Congress, Optical Society of America*, Colorado Springs, USA, pp. BW2E.7, 2012.

[17] G. Wang, U. Habib, Z. Yan, N. J. Gomes, Q. Sui, J. Wang, L. Zhang, and C. Wang, "Highly efficient optical beam steering using an in-fiber diffraction grating for full duplex indoor optical wireless communication," *J. Lightwave Technol.*, vol. 36, no. 19, pp. 4618-4625, 2018.

[18] G. Wang, C. Wang, Z. Yan, L. Zhang, "Highly efficient spectrally encoded imaging using a 45° tilted fiber grating," *Opt. Lett.*, vol. 41, no. 11, pp. 2398-2401, 2016.

[19] S. Remund, A. Bossen, X. Chen, L. Wang, A. Adebayo, L. Zhang, B. Považay, and C. Meier, "Cost-effective optical coherence tomography spectrometer based on a tilted fiber Bragg grating," in *Proc. SPIE*, 2014, pp. 89381E-89381E-8.

[20] T. Erdogan and J. Sipe, "Tilted fiber phase gratings," *J. Opt. Soc. Am. A*, vol. 13, no. 2, pp. 296-313, 1996.

[21] T. Erdogan and J. E. Sipe. "Radiation-mode coupling loss in tilted fiber phase gratings." *Opt. Lett.* vol. 20, no. 18, pp. 1838-1840, 1995.

[22] M. J. Holmes, R. Kashyap, and R. Wyatt, "Physical properties of optical fiber sidetap grating filters: Free-space model," *IEEE J. Sel. Top. Quantum Electron.*, vol. 5, no. 5, pp. 1353-1365, 1999.

[23] Y. Li, M. Froggatt, and T. Erdogan, "Volume current method for analysis of tilted fiber gratings," *J. Lightwave Technol*., vol. 19, no. 10, pp. 1580-1591, 2001.

[24] Y. Li and T. G. Brown, "Radiation modes and tilted fiber gratings," J. Opt. Soc. Am. B: Opt. Phys., vol. 23, no. 8, pp. 1544-1555, 2006.

[25] R. B. Walker, J. M. Stephen, P. Lu, and D. Grobnic, "Shaping the radiation field of tilted fiber Bragg gratings." *JOSA B*, vol. 22, no. 5, pp.962-974, 2005.

[26] C. Jáuregui and J. López-Higuera, "Near‐field theoretical model of radiation from a uniform‐tilted fiber‐Bragg grating," *Microw. Opt. Techn. Let.*, vol. 37, no. 2, pp. 124-127, 2003.

[27] C .Jauregui, A .Cobo, and J .M .Lopez-Higuera, "3D near-field model for uniform slanted fiber gratings, " *Microw. Opt. Techn. Let.*, vol. 38, no. 5, pp. 428-432, 2003.

[28] S. Lu, O. Xu, S. Feng, and S. Jian, "Analysis of radiation-mode coupling in reflective and transmissive tilted fiber Bragg gratings," *JOSA A*, vol. 26, pp. 91-98, 2009.

[29] Y. Lu, W. Huang, and S. Jian, "Full vector complex coupled mode theory for tilted fiber gratings," *Opt Express*, vol. 18, no. 2, pp. 713-726, 2010.

[30] T. Yoshino, "Theoretical analysis of a tilted fiber grating polarizer by the beam tracing approach," *JOSA B*, vol. 29, pp. 2478-2483, 2012.

[31] C. Shen, L. Xiong, A. Bialiayeu, Y. Zhang, and J. Albert. "Polarization-resolved near-and far-field radiation from near-infrared tilted fiber Bragg gratings." *J. Lightwave Technol.,* vol. 32, no. 11, pp. 2157-2162, 2014